0254-6124/2014/34(5)-757–08 *Chin. J. Space Sci.* 空间科学学报

Wang Yuren, Dai Guoliang, Wang Jing, Feng Shaobo, Luo Xinghong, Zhou Yanfei, Chen Lidong, Yu Yude. Microgravity material research in China: 2012–2014. *Chin. J. Space Sci.*, 2014, **34**(5): 757-764, doi:10.11728/cjss2014.05.757

Microgravity Material Research in China: 2012–2014

WANG Yuren[1] DAI Guoliang[1] WANG Jing[1] FENG Shaobo[2]
LUO Xinghong[2] ZHOU Yanfei[3] CHEN Lidong[3] YU Yude[4]

1(*National Microgravity Laboratory, Institute of Mechanics, Chinese Academy of Sciences, Beijing* 100190)

2(*Institute of Metal Research, Chinese Academy of Sciences, Shenyang* 110016)

3(*Shanghai Institute of Ceramics, Chinese Academy of Sciences, Shanghai* 200050)

4(*National Key Laboratory for Optoelectronic Integration, Institute of Semiconductors, Chinese Academy of Sciences, Beijing* 100083)

Abstract During 2012–2014, the main research activities from microgravity material research were focused on, which include study of microgravity effects on collagen fibrillogenesis and HAP crystallization, microgravity experiments using drop tube, and research of thermoelectric materials for space. This paper summarizes all these activities.

Key words Collagen fibrillogenesis, Crystallization, Microgravity, Refractory alloy, Facility

Classified index V 527

1 Effect of Microgravity Effect on Collagen Fibrillogenesis and HAP Crystallization

Bone loss during long-term space flight is a serious problem. It was found that over a period of 8 months in space, bone mass loss of an astronaut lost was as much as that of persons between ages 50 and 60[1].

Hydroxyapatite (HAP) crystals are the main constituents of bone. The results by Fabio *et al.* showed that collagen fibrils were key factors of HAP crystallization[2]. Therefore, HAP crystallization process will be changed if collagen fibrillogenesis changes. Collagen fibrillogenesis is a self-assembly process, which usually is expressed by diffusion-limited aggregation (DLA)[3−4]. However, the collagen clusters formed during fibrillogenesis under normal gravity are influenced by gravity and caused gravity sedimentation[5−6]. We assume that the reason of bone mass loss under microgravity conditions is the change of collagen fibrillogenesis and relevant changes of HAP crystallization process. To clarify such assumption, one needs to know the changes of collagen fibrils and HAP crystals under normal gravity ($1\,g$) and simulated microgravity (μg) conditions on the Earth. For this purpose, we prepared three-dimensional collagen fibrils and cultured HAP crystal on such collagen fibrils under $1\,g$ and simulated μg conditions. Then we observed the changes of morphology of three-dimensional collagen fibrils and HAP crystals.

1.1 Experiments

(i) Three-dimensional collagen fibrils were prepared using Type I collagen from rat tail (Sigma Co., 9007-34-5). 5 mL Collagen solution at final concentrations $3.0\,\mathrm{mg{\cdot}mL^{-1}}$ was prepared. The solution was com-

Received July 15, 2014
E-mail: yudeyu@semi.ac.cn

posed of (i) 20% collagen-Acetic acid solution, (ii) 69% H_2O, (iii) 10% 10 × MEM (Gibco Co., 41500-034), and (iv) 1.2% 0.1 M NaOH to neutralize the pH. All of the chemical reagents were analytically pure.

(ii) Simulated μg condition was achieved by three dimensional clinostat. Collagen solutions at final concentration 3.0 mg·mL^{-1} were divided into two groups. Collagen solutions in group 1 were placed into a three dimensional clinostat for 30 minutes with rotation speed of 15 rpm at 20°C. Collagen solutions in group 2 were placed into biochemical incubator at 20°C for 30 minutes. Collagen fibrillation process finished during 30 minutes. Collagen fibrils in group 1 and 2 were prepared under simulated μg and 1 g conditions, respectively.

(iii) HAP crystallization was conducted at 37.0°C. Crystallization solution was 1.5 × SBF (simulated body fluid, pH = 7.4), which was prepared according to Ref. [6]. The collagen fibrils were immersed into HAP crystal growth solution for 24 hours incubation. After that, collagen fibrils samples were taken out and frozen dried before SEM observation.

1.2 Results and Discussion

Figure 1 showed the morphology of three-dimensional collagen fibrils, which were fiberized under simulated μg (a) and 1 g (b) conditions, respectively. The amounts of cavitation in Figure 1(a) are obviously larger than that in Figure 1(b). The diameters of collagen fibrils in Figure 1(a) are much smaller than that in Figure 1(b). These results indicate that both the framework of three-dimensional and the shape of collagen fibrils are obviously different when collagen fibrillogenesis is conducted under different gravity. The effect of simulated μg was to make the framework of collagen fibrils to be more loosed and decrease the diameter of collagen fibrils. Such μg effect affects the HAP crystallization process, which is showed in Figure 2. In Figure 2(a), the shape of HAP crystals is cubic under simulated μg condition. However, most of the HAP crystals are plate-like under 1 g condition, which is showed in Figure 2(b). Under 1 g gravity, because of the bigger size and larger amount of collagen fibrils, the amounts of nucleation sites for HAP crystallization are much larger than that under μg condition. This is the reason of such difference of HAP morphology under different gravity.

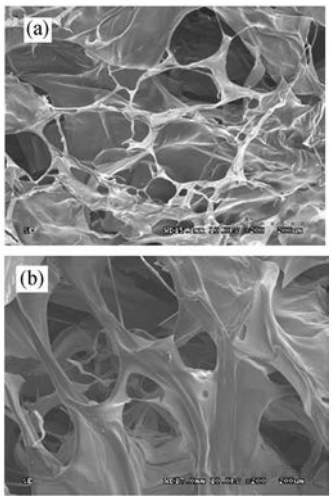

Fig. 1 Morphology of three-dimensional collagen fibrils, which were fiberized under simulated μg (a) and 1 g (b) conditions, respectively. Scale bar: 200 μm

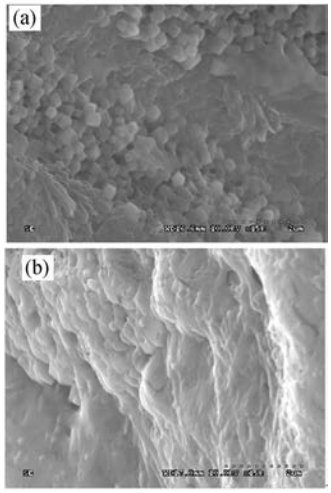

Fig. 2 Morphology of three-dimensional collagen fibrils, which were fiberized under simulated μg (a) and 1 g (b) conditions, respectively. Scale bar: 2 μm

1.3 Conclusions

The microgravity conditions obviously affect collagen fibrillogenesis, and microgravity thus affects the growth and morphology of HAP crystals. This result will help us to find ways to understand bone loss mechanism in space condition.

2 Microgravity Material Research Activities on Drop Tube

During alloy solidification, the gravity-driven convection influences heat and mass transfer, which in turn affects the solidification microstructures[9−11]. Therefore, in order to understand the fundamental physical principles governing the dendritic and eutectic microstructure formation in the diffusive and convective regime, we have performed a series of microgravity experiments using drop tube in recent years, additionally some other microgravity investigations have also been proposed or are currently in development[12].

The microgravity experiments were carried out in an evacuated 50-meter-long drop tube. During experiments, the upper half part of cylindrical samples, which were enveloped in high purity corundum crucibles, were melted by an induction heater at the top of the drop tube. Then they were released and dropped down under vacuum in the tube when given temperatures were reached, subjecting to a microgravity conditions for 3.24 s. The samples were finally quenched into silicone oil when landing at the bottom of the drop tube. For comparison, the same procedures without free falling, *i.e.*, melting and quenching, were performed on same samples in the drop tube. These samples were referred to as μg samples and $1\,g$ samples, respectively. This method was applied to investigate the influence of gravity on the dendrite growth of Ni-Al, Ni-Ti, Ni-Co, Ni-W alloys and SRR99 Ni-based single crystal superalloy, and on the growth of Al-Al_2Cu, Fe-Fe_2Ti and Al-Al_3Ni eutectic alloys. Here we report some results about Ni-based superalloy and Al-Al_3Ni alloy.

Figure 3 shows the as-solidified macrostructures of SRR99 alloy under microgravity and normal gravity conditions, respectively. The coarse dendrites on the lower part are the seed crystal. At the melting interface, columnar dendrites grow epitaxially from the seed crystal. Besides, some other dendrites nucleate at the surface of the sample and grow toward the inside, which interfere with the epitaxial growth of the dendrites from the seeds. Because the epitaxial growth of the columnar dendrites in the vicinity of the initial growth interface surely proceed during free falling for μg sample, the study of this work was focused mainly on this part.

The transverse microstructures of μg sample and $1\,g$ sample are shown in Figure 4. It is noted that the dendrite trunks are fine in both samples. The measured primary and secondary dendrite arm spacing at different distances from the melting interface is shown in Figure 5. The primary arm spacing of both samples increase with the distance away from the interface, and the spacing of $1\,g$ sample which is larger than that of μg sample. The secondary arm spacing of μg sample is almost constant with the increase of distance away from the melting interface, while that of $1\,g$ sample increases slowly. The secondary arm spacing of μg sample is smaller than that of $1\,g$ sample at the same location.

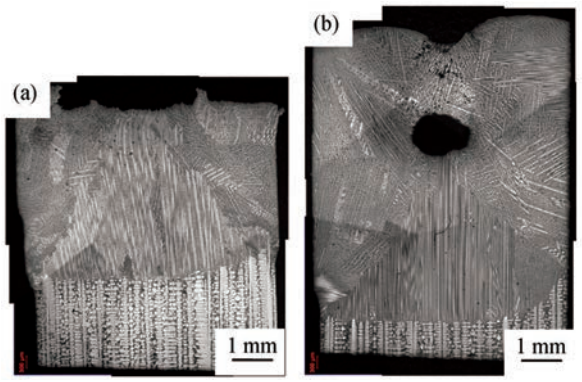

Fig. 3 Macrostructures of ingots solidified in (a) microgravity and (b) unit gravity

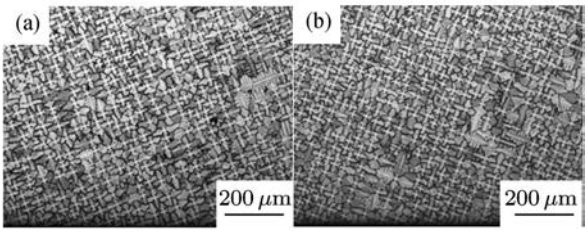

Fig. 4 Typical microstructures on transverse sections of samples solidified under (a) microgravity and (b) normal gravity

Since the cooling rate decreases gradually during solidification, the growth of some dendrite tips, for example, those behind the close dendrites, is blocked, which therefore, lead to the increase of primary arm spacing, as shown in Figure 5. Compared to μg sample, gravity-induced convection enhances the transfer of heat and mass at the front of the tips of leading dendrites, resulting in a higher growth rate of them[13]. Thus, more dendrites tips behind them stopped growing, which causes $1\,g$ sample having larger primary arm spacing. The secondary arm spacing mainly depends on the local solidification in mushy zone. Since the microscope convection in the mushy zone will increase the solute transport, and therefore increase the growth rate of secondary arms, the secondary arm spacing of $1\,g$ sample become larger compared with that of μg sample.

The influence of gravity on the growth of eutectic microstructures was studied in a similar way. Al-Al_3Ni eutectic alloy was solidified with a series of solidification parameters under both microgravity and normal gravity. Figure 6 shows the microstructures of μg sample and $1\,g$ sample, respectively. It shows that the microstructures of both μg samples and $1\,g$ samples are composed of α-Al phase matrix and regularly arrayed rod-like Al_3Ni phase. The inter-rod spacing distributions of Al_3Ni phase were determined by individually measuring the distances between each nearest neighbor rods, and the results are shown in Figure 7. It indicates that the inter-rod spacing distribution peak value and range of μg sample are larger than those of $1\,g$ sample at same growth rate. In addition, the spacing distribution peak values and ranges under both conditions decrease gradually with the increase of solidification velocity. Furthermore, from Figure 8 which shows the trend of change of average eutectic spacing with growth rate, it can be found that, with the growth rate increasing, the difference between the average spacing under the two gravity levels reduces gradually, even though they both reduce gradually and the average spacing under μg is always larger than that under $1\,g$.

During the coupled growth of the Al-Al_3Ni eutectic, under the effect of diffusion, Al and Ni elements would segregate separately at the fronts of α-Al phase and Al-Al_3Ni phase. This would lead to local element enrichment in the solute boundary layer, and correspondingly, change the local melt density. Under the influence of buoyancy convection, the melt rich in Al, which is lighter than the homogenous melt ahead of the growth front, would move up. As a result, Ni concentration in the solute boundary layer would go up, and consequently, the eutectic spacing has to get closer to keep phase equilibrium. While under μg condition, no buoyancy convection exists any more, the eutectic spacing would be selected by a nearly pure diffusion process. Besides, due to the rise of Ni concentration in the solute boundary layer, the effective diffusion coefficient under normal gravity becomes larger. To validate the hypothesis, the Al

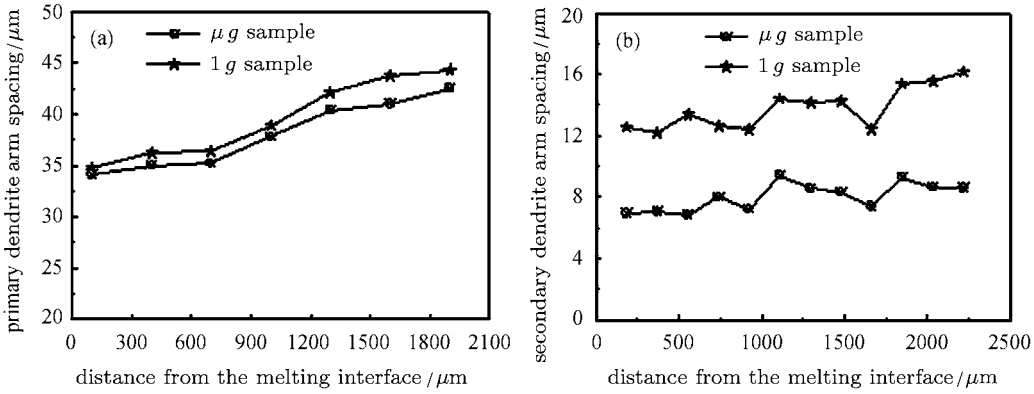

Fig. 5 Primary (a) and secondary (b) dendrite arm spacing at different locations in μg sample and $1\,g$ sample

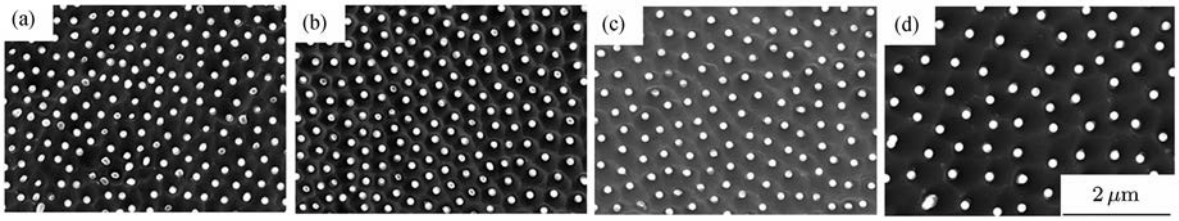

Fig. 6 SEM images showing the cross section microstructures of the samples grown at $V = 1912\,\mu\text{m}\cdot\text{s}^{-1}$ under (a) $1\,g$ and (b) μg, $V = 1075\,\mu\text{m}\cdot\text{s}^{-1}$ under (c) $1\,g$ and (d) μg, respectively

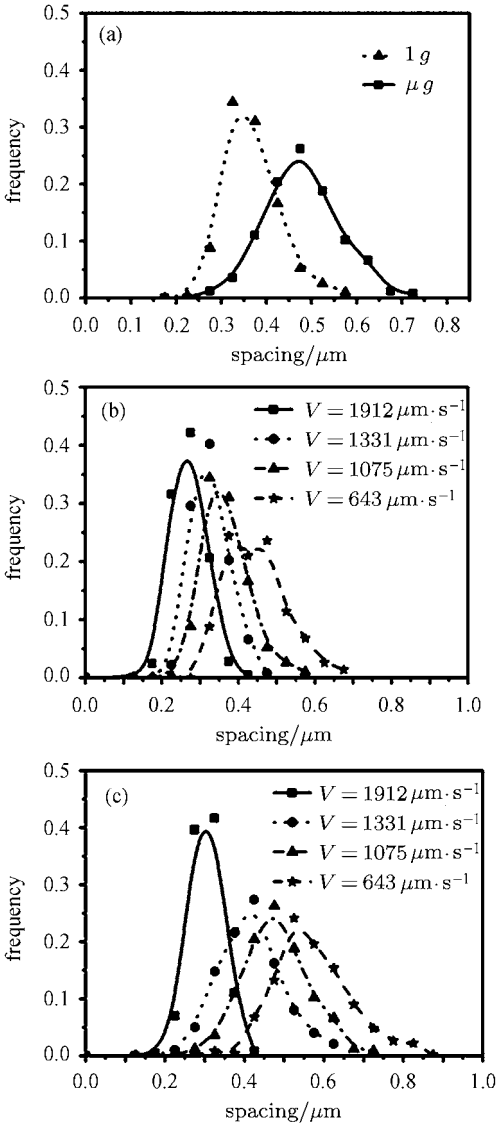

Fig. 7 (a) Effect of gravity level on eutectic spacing distribution at $V = 1075\,\mu\text{m}\cdot\text{s}^{-1}$ and effect of growth rate on eutectic spacing distribution under (b) $1\,g$ and (c) μg

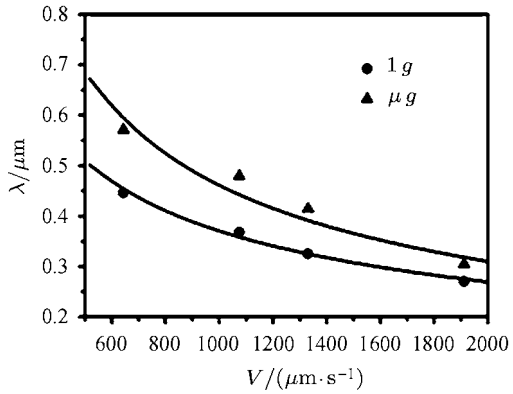

Fig. 8 Change of the average eutectic spacing with growth rate

contents at different distances along the growth direction within zone B in each sample are determined by EDAX, and the result (Figure 9) shows that the Al contents increase with growth proceeding upwards in every $1\,g$ sample, while those in μg samples keeps almost unchanged.

It can also be observed in this work that the effect of buoyancy convection on the eutectic spacing is closely related with dynamic factors, such as growth rate. With acceleration growth, the differences of eutectic spacing and Ni content at the same growth section between $1\,g$ and mg samples are both diminishing. This is proved by experiment that only when growth rate is smaller than convection rate, convections driven by gravity play an important role in the formation of eutectic solidification microstructure, and larger the difference between the growth rate and convection rate, more important role gravity will play. It can be estimated that once the growth

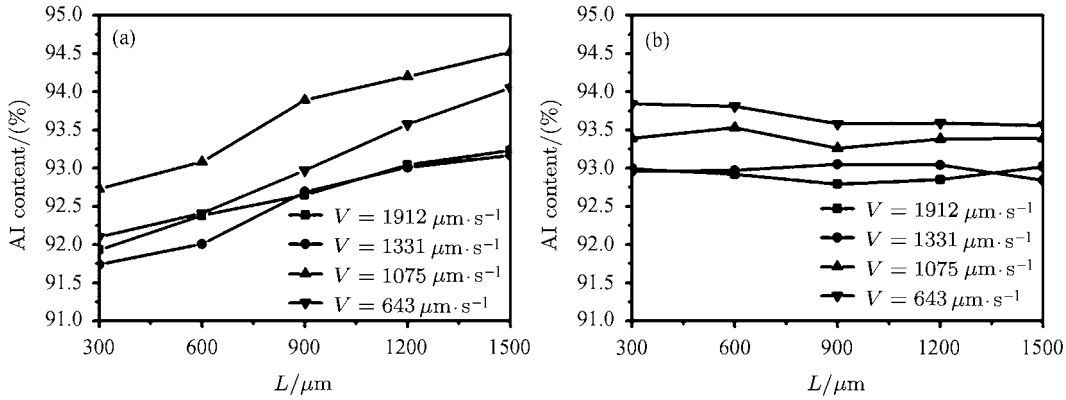

Fig. 9 Al content distribution along the growth direction in (a) $1\,g$ samples and (b) μg samples

rate go beyond the convection rate, gravity convection will have no effect on the solidification microstructure any more.

3 Research of Thermoelectric Materials for Space

Thermoelectric conversion has attracted much interest for the application in electronic cooling, waste heat recovery and space power source, because it is silent in operation and highly reliable with no moving parts as well as long operation life when installed at any angle[14−15]. The conversion efficiency of thermoelectric devices is greatly related with the figure-of-merit (ZT) of thermoelectric materials and temperature difference. As for a given thermoelectric material system, the chemical composition and microstructure is a major factor influencing the thermoelectric performance. There are many types of thermoelectric materials, which can be divided into three categories according to the working temperature. Bi_2Te_3-based alloys are well-known as the best Peltier cooling materials currently used near room temperature and good power generation materials at about 250°C[16−17]. Doped or filled $CoSb_3$-based skutterudite compounds have high ZT values and are regarded as one of the promising materials working at medial temperature range[18−21]. $CoSb_3$-Bi_2Te_3-based cascade components and integrated systems are currently being developed to support the future deep space exploration missions.

3.1 Results of Space Experiment of $Bi_2Se_{0.21}Te_{2.79}$ Crystal

In space microgravity environment, the buoyancy-driven convection, sedimentation and hydrostatic pressures in the process of crystal growth can be validly suppressed, therefore compositional homogeneity and structural integrity can be improved greatly. The n-type $Bi_2Se_{0.21}Te_{2.79}$ crystal was grown under microgravity conditions by zone melting on the Foton-M3 spacecraft of Russia in 2007[22]. The distribution of chemical composition along growth direction and XRD results show that compositional homogeneity and crystallization of space-grown crystal are obviously improved. The highest ZT values of 1.14 and 0.88 are obtained at 300 K for space- and ground-grown crystals along crystal growth direction, respectively. The ZT value of space-grown crystal is higher than that of ground-grown crystal in the temperature range 300–500 K, suggesting that high crystallization under microgravity conditions is beneficial to Bi_2Te_3-based thermoelectric materials.

3.2 Ground-based Research of Thermoelectric Materials

In order to understand the inherent law of the solute transport of multi-component system in the process of crystal growth, and to reveal the influence of compositional and micro-structural change of thermoele-

Fig. 10 Product photo of a $Bi_{0.52}Sb_{1.48}Te_3$ ampoule

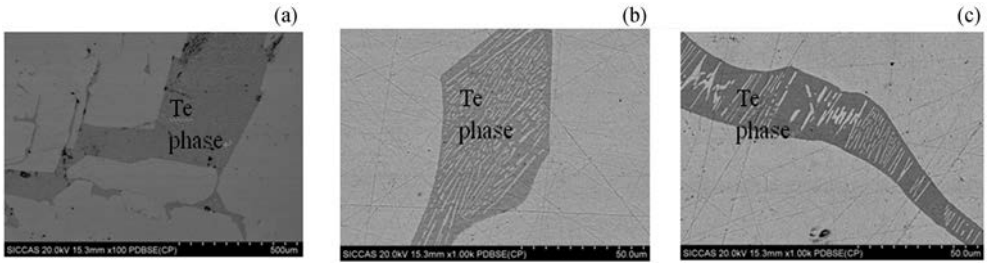

Fig. 11 Scanning electron microscopy images for $Bi_{0.52}Sb_{1.48}Te_3$samples grown at the rate of (a) $3\,mm{\cdot}h^{-1}$, (b) $5\,mm{\cdot}h^{-1}$, and (c) $7\,mm{\cdot}h^{-1}$

ctric material on thermoelectric transport properties, the crystal of p-type $Bi_{0.52}Sb_{1.48}Te_3$ is planning to be grown on Tiangong-2 target spacecraft. A series of ground experiment has been carried out since 2011. Figure 10 shows a quartz crucible for $Bi_{0.52}Sb_{1.48}Te_3$, which is made of two-double quartz structure. The total length of the ampoule is 260 ± 0.2 mm and the diameter of the ampoule is 16–0.2 mm. The dimension of $Bi_{0.52}Sb_{1.48}Te_3$ ingot in the ampoule is $7.6\pm$ 0.2 mm in diameter and $55\pm$ 0.2 mm in length. The $Bi_{0.52}Sb_{1.48}Te_3$ ampoule has to withstand the vibration and shock test required by Tiangong-2 target spacecraft.

In order to determine the best technological parameters of space experiments, we investigated the influence of sample growth rate on thermoelectric performance. When keeping other conditions unchanged, typical microstructures of the samples grown by different growth rate $3\,mm{\cdot}h^{-1}$, $5\,mm{\cdot}h^{-1}$ and $7\,mm{\cdot}h^{-1}$ are shown in Figure 11. The analysis of samples by scanning electron microscope (SEM) shows that there is Te precipitate phase and its amount decreases with increasing sample growth rate. The existence of Te phase is equivalent to the donor doping in the Bi-Sb-Te system. The results show that the hole concentration increases with the decrease of extra Te content, and thus increases electrical conductivity and decreases scattering on phonons. The influence of growth rate on the thermoelectric performance is showed in Figure 12. The maximum ZT value of 1.04 is obtained at 350 K for $5\,mm{\cdot}h^{-1}$ velocity. The growth rate of $5\,mm{\cdot}h^{-1}$ is determined as most appropriate one for $Bi_{0.52}Sb_{1.48}Te_3$ samples.

High performance $CoSb_3$-based skutterudites and $CoSb_3/Bi_2Te_3$-based segment materials can greatly improve energy conversion efficiency of thermoelectric power generator. We carried out studies on $CoSb_3$-based skutterudites and $CoSb_3/Bi_2Te_3$-based materials and devices. Skutterudites with multiple fillers Ba, La and Yb were synthesized and very high thermoelectric figure of merit ZT = 1.7 at 850 K

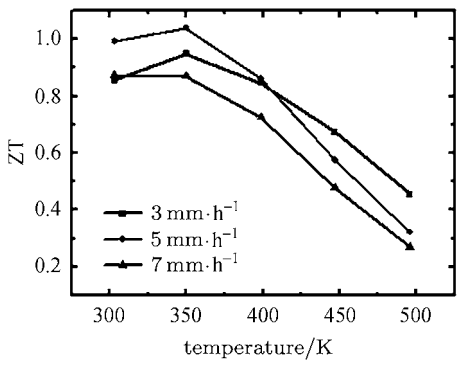

Fig. 12 Temperature dependence of ZT for $Bi_{0.52}Sb_{1.48}Te_3$ samples grown at $3\,mm{\cdot}h^{-1}$, $5\,mm{\cdot}h^{-1}$ and $7\,mm{\cdot}h^{-1}$

was obtained[23], which is the highest value reported in skutterudites. We have developed process for scaling up skutterudites and the ZT value reached 1.35 at 850 K for the scaled skutterudite materials. We have also developed electrode and integrating technology for the skutterudite devices, and the energy conversion efficiency of the skutterudite devices and the $CoSb_3/Bi_2Te_3$-based cascade devices can reach 8.2% and 10.1%, respectively.

References

[1] Liu X Y. Effect of microgravity on Ca mineral crystallization and implications for osteoporosis in space [J]. *Appl. Phys. Lett.*, 2001, **79**:35-39

[2] Fabio N, Koen P, Anne G, *et al.* The role of collagen in bone apatite formation in the presence of hydroxyapatite nucleation inhibitors [J]. *Nat. Mat.*, 2010, **9**:1004-1009

[3] John P, Karl E, Brass A. Simple physical model of collagen fibrillogenesis based on diffusion limited aggregation [J]. *J. Mol. Biol.*, 1994, **247**:823-831

[4] John P, Karl E, Andy B. Self-assembly of rodlike particles in two dimensions: A simple model for collagen fibrillogenesis [J]. *Phys. Rev.*, 1994, **50**:2963-2966

[5] Sedgwick H, Egelhaaf S U, Poon W C K. Clusters and gels in systems of sticky particles [J]. *J. Phys.*, 2004, **16**:S4913-S4922

[6] Jonathan K W, Erik L. Sedimentation of aggregating colloids [J]. *J. Chem. Phys.*, 2011, **134**:034510

[7] Oyane A, Kim H M, Furuya T, *et al.* Preparation and assessment of revised simulated body ?uids [J]. *J. Biom. Mat. Res.*, 2002, **65**:188-195

[8] Vergara A, Lorber B, Zagari A, *et al.* Physical aspects of protein crystal growth investigated with the advanced protein crystallization facility in reduced-gravity environments [J]. *Acta Cryst. D*, 2003, **59**:2

[9] Mirihanage W U, Browne D J, Sturz L, Zimmermann G. A combined enthalpy/front tracking method for modeling melting and solidification in laser welding [C]//3rd International Conference on Advances in Solidification Processes, 2012: 27

[10] Hainke M, Steinbach S, Ratke L, Muller G. The effect of forced fluid flow on microstructure in directionally solidified Al-Si-base alloys [J]. *Trans. Indian Inst. Metals*, 2005, **58**:639-644

[11] Thi H N, Dabo Y, Drevet B, *et al.* Chilton Directional solidification of Al-1.5 wt % Ni alloys under diffusion transport in space and fluid-flow localisation on Earth [J]. *J. Cryst. Growth*, 2005, **281**:654-668

[12] Feng S B, Luo X H. Investigation of growth of single crystal SRR99 superalloy under microgravity using 50-meterhigh drop tube [C]//International Symposium on Physical Sciences in Space, 2011: 327

[13] Ratke L, Genau A, Steinbach S. Flow effects on the dendritic microstructure of AlSi-base alloys [J]. *Trans. Indian Inst. Metals*, 2009, **62**:337-341

[14] Disalvo F J. Thermoelectric Cooling and Power Generation [J]. *Science*, 1999, **285**:703-706

[15] Funahashi R, Mikami M, Mihare T, Urata S, Ando N. A portable thermoelectric-power-generating module composed of oxide devices [J]. *J. Appl. Phys.*, 2006, **99**:066117

[16] Jiang Y P, Jia X P, Su T C, Dong N, Ma H A. Thermoelectric properties of SmxCo4Sb12 prepared by high pressure and high temperature [J]. *J. Alloys compd.*, 2011, **493**:535

[17] Majumdar A. Thermoelectricity in semiconductor nanostructures [J]. *Science*, 2004, **303**:777-778

[18] Bai S Q, Pei Y Z, Chen L D, Zhang W Q. Enhanced thermoelectric performance of dual-element-filled skutterudites BaxCeyCo4Sb12 [J]. *Acta Mater.*, 2009, **57**:3135

[19] Zhang J J, Xu B, Yu F R, Yu D L, Liu Z Y, He J L, Tian Y J. Thermoelectric properties of n-type CoSb3 fabricated with high pressure sintering [J]. *J. Alloys Compd.*, 2010, **503**:490

[20] Zhang L, Melnychenko-Koblyuk N, Royanian E, Grytsiv A, Rogl P, Bauer E. Influence of filler element and Ni-substitution on thermoelectric properties of multi-filled skutterudites [J]. *J. Alloys Compd.*, 2010, **504**:53

[21] Xiong Z, Chen X H, Huang X Y, Bai S Q, Chen L D. High thermoelectric performance of Yb0.26Co4Sb12/yGaSb nanocomposites originating from scattering electrons of low energy [J]. *Acta Mater.*, 2010, **58**:3995

[22] Zhou Yanfei, Li Xiaoya, Bai Shengqiang, Chen Lidong. Comparison of space-and ground-grown Bi2Se0.21Te2.79 thermoelectriccrystals [J]. *J. Cryst. Growth*, 2010, **312**:775

[23] Shi Xun, Yang Jiong, Salvador J R, *et al.* Multiple-Filled Skutterudites: High Thermoelectric Figure of Merit through Separately Optimizing Electrical and Thermal Transports [J]. *J. Am. Chem. Soci.*, 2011, **133**:7837